Supporting Information

Ma et al. 10.1073/pnas.1117491109

SI Materials and Methods

Mice and Imaging Experiment. The *OMP-IRES-tTA* (Jackson Laboratories stock no. 017754) and *tetO-G-CaMP2* (Jackson Laboratory stock no. 017755) mice were described previously (1, 2). The *tetO-G-CaMP2* mouse lines known as 12i and 5i, which exhibited strong fluorescence, were crossed to produce animals for this study. The compound heterozygotes were further crossed to *P2-IRES-tauLacZ* (Jackson Laboratory stock no. 006595) and *MOR28-IRES-EGFP* lines (2, 3). Animals were maintained in the Lab Animal Services Facility of Stowers Institute at 12-h:12-h light/dark cycle and provided with food and water ad libitum. Experimental protocols were approved by the Institutional Animal Care and Use Committee at Stowers Institute and were in compliance with the National Institutes of Health Guide for Care and Use of Animals.

Odor Delivery. An olfactometer was constructed according to the design of Uchida and Mainen (4). Odor delivery was computer controlled with a custom-written software package developed using LabView (National Instruments). Odorants were freshly diluted in mineral oil on the day of the experiment and used within 24 h. Saturated odor vapor from each vial was diluted into a carrier stream of clean air through a manifold. Four mass flow controllers were used to maintain the flow rate of clean air and odor vapor via different channels. The total flow rate was maintained at 400 mL/min. Odor output was measured by a photo ionization detector (Aurora Scientific) before each experiment. Measured concentrations corresponded linearly with liquid dilution in the vials from 3×10^{-3} to 10^{-1} dilutions, consistent with previous observations (5). Odor concentrations were thus presented as percentage of saturated vapor calculated from liquid dilution and air dilution. Odor delivery time was 2 s, and odor sequence was randomized. Each odor was delivered from the lowest to the highest concentration in a sequence, with an 8- to 10-s interstimulus interval. An interval of more than 3 min is imposed before the next odor sequence. A subset of odors was delivered multiple times at random intervals to test the consistency of the responses. Other odors were delivered once for each concentration. In experiments shown in Fig. S8, multiple odors at 2.5% saturated vapor (S.V.) were delivered sequentially with an interstimulus interval of 10 s. Chemicals were purchased from Sigma-Aldrich or obtained as samples from International Flavors & Fragrances.

Optical Imaging. Two- to six-month-old G-CaMP2 mice were anesthetized by urethane, and the bone covering the olfactory bulb was thinned with dental tools. Odor responses were recorded by a Hamamatsu EM-CCD camera mounted on an Olympus BX50WI microscope using 2.5× (0.15 N.A.), 4× (0.10 N.A.), or 5× (0.25 N.A.) objectives. The frame rate was 8.5 Hz for image acquisition. A Xenon short arc XBO light source passed through a band-pass filter (450–490 nm; Olympus America) was used to excite the dorsal olfactory bulb. Images were binned 2×2, and the image size was 256×256 pixels.

Image Analysis. Imaging data analysis was performed using ImageJ (National Institutes of Health) with custom-written Java scripts to assist batch processing of the image files. To identify the activated glomeruli, all image stacks from the one experiment were aligned to an arbitrarily selected standard stack from the same experiment. The activated glomeruli were revealed by subtracting minimally projected background images from the aligned stack. Discrete areas corresponding to individual glomeruli were manually identified as regions of interest (ROIs). To identify all responding glomeruli in one experiment, the activated areas were compared across all odor stimuli. If an area responded to odor stimuli with consistent spatial and temporal patterns, it was considered as a single glomerulus. The maximal size of a ROI was set to be at 100 μm in diameter. ROIs obtained from all odor stimulations were pooled together to obtain a master ROI list. Measurement of response was performed on aligned image stacks without background subtraction to reflect the true ΔF/F. Mean pixel values of each ROI were used for analyses.

Data Analysis. A custom-written software package developed in MATLAB was used for signal processing and subsequent data analysis. The raw data trace was smoothed and baseline adjusted to obtain a ΔF/F trace. A peak-finding algorithm from a MATLAB package (http://terpconnect.umd.edu/~toh/spectrum/PeakFindingandMeasurement.htm) was implemented to automatically identify response peaks. The peak values were used for further analysis.

In chemotopic analyses, the peak responses of individual glomerulus to a specific odor were mapped to its locations. For analyses on odor groups, the maximal peak response to all odors within the odor group was used and mapped to the glomerular positions. For statistical test of the chemotopy hypothesis, the mean distance between two sets of glomeruli was calculated as:

$$d_{ij} = \frac{\sum_p \sum_q \sqrt{(x_{ip} - x_{jq})^2 + (y_{ip} - y_{jq})^2}}{i * j},$$

where d_{ij} denotes the average glomerulus distance between two glomerular sets activated by odor i and odor j; x and y denote the coordinates of the activated glomerulus; p denotes the activated glomerulus for odor i, and q denotes the activated glomerulus for odor j.

The odorant pairs were segregated into two groups: WITHIN group for odor pairs belonging to the same chemical class and the BETWEEN group for two odors belonging to different chemical classes. The chemotopy hypothesis was expressed as:

$d\_\text{BETWEEN} - d\_\text{WITHIN} \geq D$, where D was the distance at which chemotopy was considered to exist.

Odor tuning similarity is calculated as:

$$Sij = \sum_m r_{im} * r_{jm} \Big/ \sqrt{\sum_m r_{jm}^2 \sum_m r_{im}^2}.$$

Distance for the two glomeruli was expressed as $Dij = 1 - Sij$, where i and j denote the identity of the glomerulus and r_{im}, and r_{jm} corresponds to the peak amplitude to mth odor for the two glomeruli. Similar calculation was used for calculating distance between two odor-evoked activity patterns, with r_{im} and r_{jm} corresponding to the response of the mth glomerulus to odors i and j. Euclidean distance measurements gave rise to qualitatively the same conclusions. Cluster analysis and PCA were performed using the MATLAB Statistics Toolbox. PCA was performed with the z score of the response amplitude.

Pairwise analysis of glomerular response similarity and physical distance. Pairwise glomeruli similarity value *Sij* was plotted against the physical distance between the glomerular pair. Only pairs of glomeruli in the same olfactory bulb were used. Similarity scores were calculated using responses across all concentrations unless

otherwise stated. By projecting the distribution of the scatter plot onto either axis, we obtained the marginal distribution of similarity and distance. Joint distribution of the two marginal distributions was calculated to show the expected result under the null hypothesis that similarity and distance were independent of each other. Difference between the actual and the null hypothesis distributions was calculated by subtracting the null hypothesis distribution from the actual.

Comparison between glomeruli responses and odor descriptors. Odors were expressed as vectors in odor space defined by the chemical descriptors (6, 7) or by the peak responses of a common set of glomeruli. Responses from the same animal to the same odorant at all concentrations were concatenated to form a single vector. In the descriptor representation, an odor was represented by either the full set of 1,664 descriptors or the two optimized subsets of 20 or 40 descriptors (6, 7).

Similarities were calculated using Pearson correlation value for the two representations. Pairwise response similarity vs. odor space distance was plotted for all odor pairs.

Fisher's Combined Test of Chemotopy for Data in the Dorsal Bulb. For each olfactory bulb, an individual probability p was obtained from two-sample t test. To combine results from all bulbs, Fisher's combined probability test was used to integrate extreme value probabilities into the χ^2 statistic as:

$$X^2 = \sum_{i=0}^{k} \log_e(p_i). \qquad \textbf{[S1]}$$

Then the overall P value was calculated from the χ^2 distribution with degree of freedom as 2k; k is the number of tests combined (12 total).

Test of Chemotopy for the Entire Olfactory Bulb. We build a simplified model of chemotopy to perform statistical analyses. We treat the entire bulb as a sphere with all of the glomeruli residing on the surface of the sphere. We first assume that every odor class is represented by distinct regions of the sphere with no overlap. For N classes of odorants, the surface area of the sphere is evenly divided into N equal sections. The surface area of each section is

$$A_N = \frac{A_{Sphere}}{N}, \qquad \textbf{[S2]}$$

where surface area of a sphere is given by

$$A_{Sphere} = 4\pi r^2. \qquad \textbf{[S3]}$$

From our experimental results, we observed that all eight odor classes were represented in the dorsal area. We therefore consider the overlap case without changing the areas assigned to each odor class. We model each region as spherical to simplify the calculation. Consider a region that all sections overlap, with an area of $A_{overlap}$. If the area of the overlap region is included in the area of each of the sections, the total area of each odor class section becomes

$$A_N = \frac{A_{Sphere}}{N} + \frac{N-1}{N} \cdot A_{Overlap}, \qquad \textbf{[S4]}$$

where area of the overlapping region is given by

$$A_{Overlap} = Overlap\% \cdot A_{Sphere}. \qquad \textbf{[S5]}$$

In an extreme case, this situation could be visualized as a sphere cut radially into N equal sections, with a circular overlap region at the pole of the sphere shared by each section (Fig. S4*C*).

Our basic model, based on this scenario, permits us to assess the likelihood that randomly placed areas (corresponding to odor classes) will overlap in such a way. Specifically, we will take the circular overlap region to be at the pole of the sphere, then randomly place other circular regions (with the appropriate area A_N calculated above) onto the sphere and find the probability that all circular regions fully contain the overlap region (Fig. S4*C*).

In spherical coordinates, the surface area of each circular region, the area of a solid angle taken at the surface of the sphere, is given by

$$A = 2\pi r^2(1 - \cos\alpha), \qquad \textbf{[S6]}$$

where α is the angle from the center point to the edge of the area (Fig. S4*C*, *Left*). The angle α_{ov} can now be described as a function of the overlap percent by setting Eq. **S5** equal to Eq. **S6**:

$$Overlap\% \cdot A_{Sphere} = 2\pi r^2(1 - \cos\alpha_{Ov})$$

to obtain

$$\alpha_{Ov}(Overlap\%) = \cos^{-1}[1 - (2 \cdot Overlap\%)]. \qquad \textbf{[S7]}$$

Eq. **S7** gives us the angle α of the overlap region as a function of the overlap percent. We can also determine α for our other circular regions by setting Eq. **S4** equal to Eq. **S6**:

$$\frac{A_{Sphere}}{N} + \frac{N-1}{N} \cdot A_{Overlap} = 2\pi r^2(1 - \cos\alpha_{CR}),$$

where after substitutions and algebra, we obtain α as a function of the number of odor class regions N and the overlap percent *Overlap%*:

$$\alpha_{CR}(N, Overlap\%) = \cos^{-1}\left\{1 - \frac{2}{N}[1 + (N-1) \cdot Overlap\%]\right\}. \qquad \textbf{[S8]}$$

In radial coordinates where the center of each area is expressed as (r, θ, ϕ), the radius r is held constant, and any change in the azimuth angle ϕ gives identical results. Therefore, the probabilities with which an area A_N contains the overlap area $A_{Overlap}$ can be expressed in terms of θ, which describes the angular distance between the pole and A_N for the area representing a given class of odor (Fig. S4*C*). The probability of a single randomly placed odor class region fully containing the overlap region whose center is located at the sphere's pole (r, 0, 0) can be calculated when the center of the odor class region given by (r, θ, ϕ) must satisfy

$$\theta \le \alpha_{CR} - \alpha_{Ov}, \qquad \textbf{[S9]}$$

which gives rise to

$$P_1 = \frac{\alpha_{CR} - \alpha_{Ov}}{\pi}. \qquad \textbf{[S10]}$$

Therefore, the probability of N randomly placed odor class region fully containing the overlap region is

$$P_N = \left(\frac{\alpha_{CR} - \alpha_{Ov}}{\pi}\right)^N. \qquad \textbf{[S11]}$$

The probability P_N as a function of N and *Overlap%* can be calculated using Eqs. **S7**, **S8**, and **S11**.

Testing Effect of High-Concentration Odor Exposure on Correlation Between Glomerular Distance and Tuning Similarity. The overall similarity scores in our experiments (Fig. 5) are higher than those in the Soucy et al. study (8). This can be explained by the difference in probe sensitivity and the odor panels used. We have used only odors that activate the dorsal glomeruli, whereas the

calculation by Soucy et al. included many odors that did not activate the dorsal bulb. High probe sensitivity also allowed the detection of relatively weak responses. Because nonzero values in odor response vector tend to increase similarity score, the higher similarity scores observed in our study can be explained by these two factors. However, the change in score distribution could not explain the substantially stronger correlation between tuning similarity and the closeness of the glomeruli observed in our study. We reasoned that the discrepancy might be explained by the fact that our analyses used lower odor concentrations as well as a different temporal sequence of odor stimulation. Repeated, long exposures to relatively high-concentration odors, as in earlier studies (5, 8–17), might have resulted in the suppression of responses from some glomeruli. To test this conjecture, we performed experiments by sequentially exposing the animals to a panel of odors at high concentrations (2.5% s.v.). The results are shown in Fig. S8.

1. He J, Ma L, Kim S, Nakai J, Yu CR (2008) Encoding gender and individual information in the mouse vomeronasal organ. *Science* 320:535–538.
2. Yu CR, et al. (2004) Spontaneous neural activity is required for the establishment and maintenance of the olfactory sensory map. *Neuron* 42:553–566.
3. Mombaerts P, et al. (1996) Visualizing an olfactory sensory map. *Cell* 87:675–686.
4. Uchida N, Mainen ZF (2003) Speed and accuracy of olfactory discrimination in the rat. *Nat Neurosci* 6:1224–1229.
5. Meister M, Bonhoeffer T (2001) Tuning and topography in an odor map on the rat olfactory bulb. *J Neurosci* 21:1351–1360.
6. Haddad R, et al. (2008) A metric for odorant comparison. *Nat Methods* 5:425–429.
7. Saito H, Chi Q, Zhuang H, Matsunami H, Mainland JD (2009) Odor coding by a Mammalian receptor repertoire. *Sci Signal* 2:ra9.
8. Soucy ER, Albeanu DF, Fantana AL, Murthy VN, Meister M (2009) Precision and diversity in an odor map on the olfactory bulb. *Nat Neurosci* 12:210–220.
9. Johnson BA, Woo CC, Hingco EE, Pham KL, Leon M (1999) Multidimensional chemotopic responses to n-aliphatic acid odorants in the rat olfactory bulb. *J Comp Neurol* 409:529–548.
10. Johnson BA, Leon M (2000) Odorant molecular length: One aspect of the olfactory code. *J Comp Neurol* 426:330–338.
11. Johnson BA, Farahbod H, Leon M (2005) Interactions between odorant functional group and hydrocarbon structure influence activity in glomerular response modules in the rat olfactory bulb. *J Comp Neurol* 483:205–216.
12. Inaki K, Takahashi YK, Nagayama S, Mori K (2002) Molecular-feature domains with posterodorsal-anteroventral polarity in the symmetrical sensory maps of the mouse olfactory bulb: mapping of odourant-induced Zif268 expression. *Eur J Neurosci* 15: 1563–1574.
13. Uchida N, Takahashi YK, Tanifuji M, Mori K (2000) Odor maps in the mammalian olfactory bulb: Domain organization and odorant structural features. *Nat Neurosci* 3: 1035–1043.
14. Igarashi KM, Mori K (2005) Spatial representation of hydrocarbon odorants in the ventrolateral zones of the rat olfactory bulb. *J Neurophysiol* 93:1007–1019.
15. Rubin BD, Katz LC (1999) Optical imaging of odorant representations in the mammalian olfactory bulb. *Neuron* 23:499–511.
16. Takahashi YK, Kurosaki M, Hirono S, Mori K (2004) Topographic representation of odorant molecular features in the rat olfactory bulb. *J Neurophysiol* 92:2413–2427.
17. Matsumoto H, et al. (2010) Spatial arrangement of glomerular molecular-feature clusters in the odorant-receptor class domains of the mouse olfactory bulb. *J Neurophysiol* 103:3490–3500.

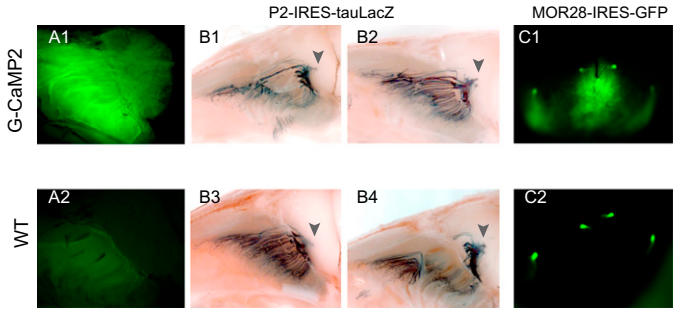

Fig. S1. Projection of OSNs in *tetO-G-CaMP2/OMP-IRES-tTA* mice. (*A*) Wide-field fluorescent images from the bisected heads of a compound heterozygote *OMP-IRES-tTA/tetO-G-CaMP2/P2-IRES-tauLacZ* mouse (*A1*) and a *P2-IRES-tauLacZ* control mouse (*A2*). In the control mouse, faint autofluorescent signal is observed in the main olfactory epithelium. (*B*) LacZ staining of the same animals. P2 OSN projections are examined from both the left and right bulbs. Images of the left bulbs are flipped to the same orientation as the right bulb. Arrowheads indicate the P2 glomeruli. (*C*) MOR28 projections are visualized in compound heterozygote *OMP-IRES-tTA/tetO-G-CaMP2/MOR28-IRES-EGFP* mouse (*C1*) and a control *MOR28-IRES-EGFP* (*C2*) mouse. Both the left and right bulbs are shown from ventral sides, with anterior part of the bulb pointing upward. The four bright green spots are the MOR28 glomeruli. *Upper Right*: Background green signals are from G-CaMP2.

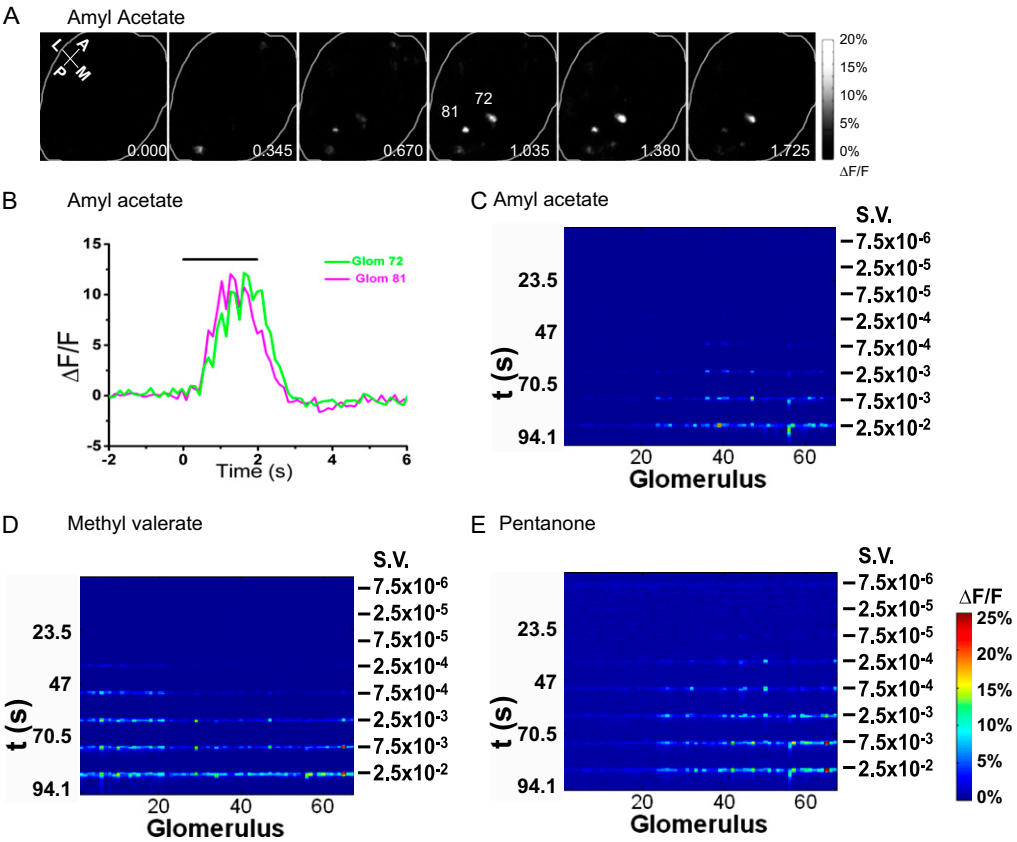

Fig. S2. Odor-evoked responses in the G-CaMP2 animals. (*A*) Image frames show the dorsal bulb response patterns during 2-s applications of the odorant amyl acetate. Six frames from image stacks are shown representing the beginning, duration, and end of the responses. The images shown are subtracted from the background fluorescence. Time stamps from the start of odor delivery (at 0 s) are indicated in the images. Image size is $1.625 \times 1.625 mm^2$. (*B*) Response trace for two glomeruli (72 and 81). The positions of the glomeruli are indicated in *A*. Duration of odor application is shown in the black bar above the traces. (*C*–*E*) The corresponding heatmaps show the ΔF/F response to amyl acetate (*C*), methyl valerate (*D*), and pentanone (*E*) for all of the glomeruli. Vertical axes indicate time. Examples shown in *C*–*E* are from a different experiment shown in *A* and *B*. The color of the pixel indicates the intensity of the response for a glomerulus.

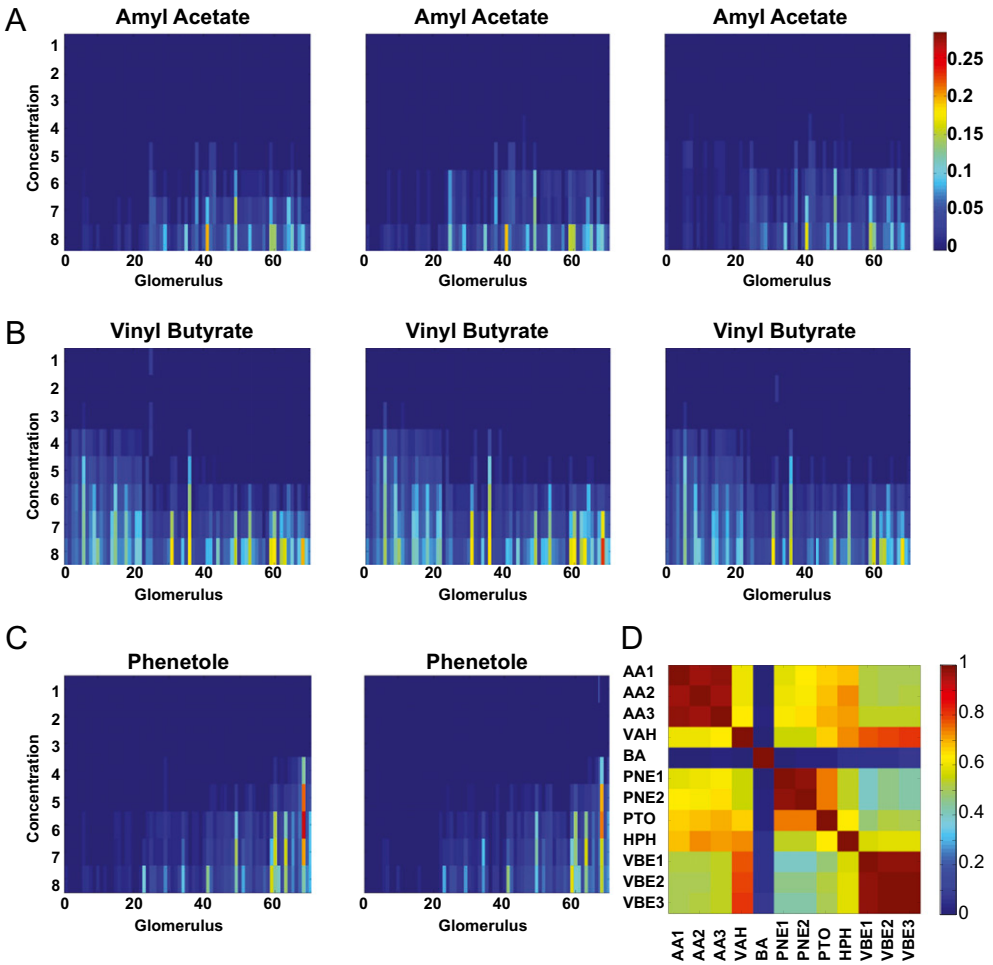

Fig. S3. Consistency in odor responses. (*A*) Heatmaps showing the peak glomerular response to three separate applications of amyl acetate (AA) at eight concentrations. Each column indicates the response from a single glomerulus, and each row indicates the response of all glomeruli to a single concentration of the odor. (*B*) Heatmap showing the peak glomerular responses to three separate applications of vinyl butyrate (VBE) at eight concentrations. (*C*) Peak glomerular response heatmaps to two separate applications of phenetole (PNE). Color bar in *A* shows the ΔF/F value for each glomerulus to each odor application. (*D*) cross-correlation among odor response patterns for the subset of odors shown. Correlation values are calculated using response from all glomeruli across the odor concentrations.

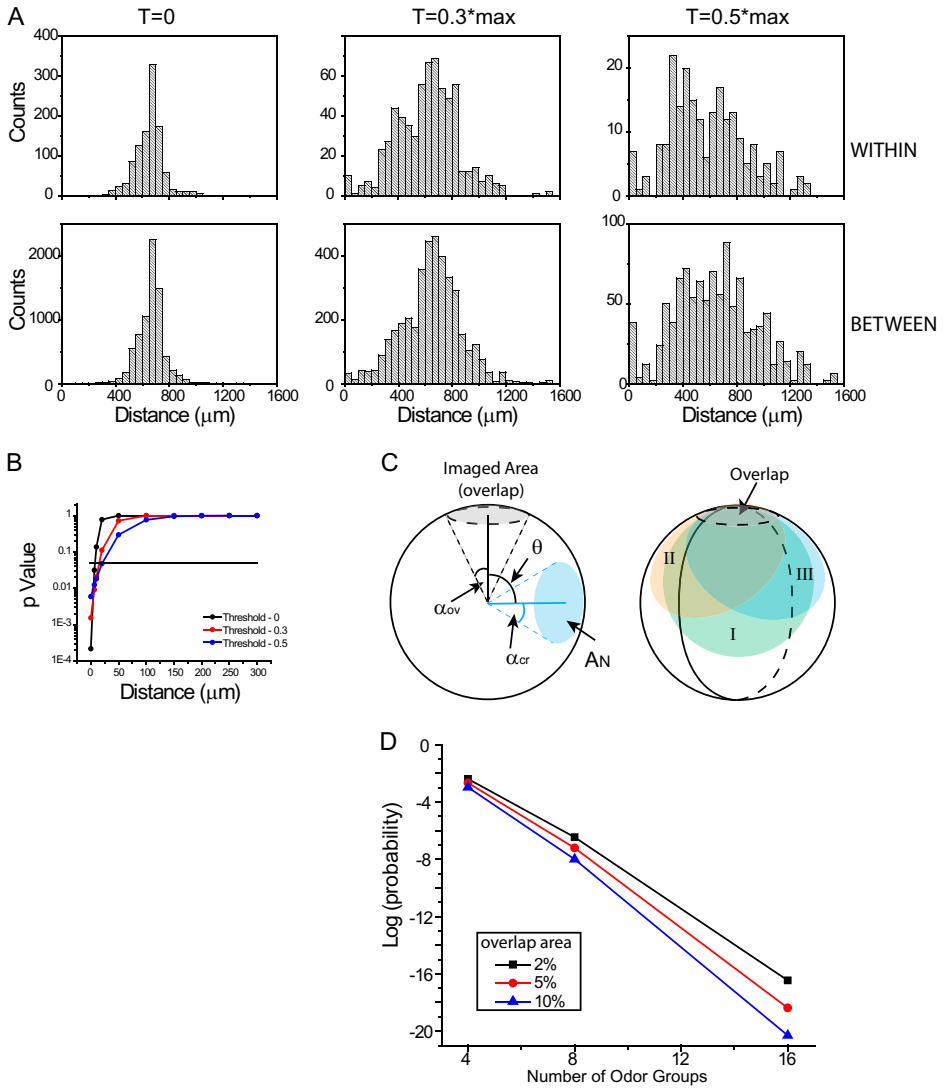

Fig. S4. Statistical test of the chemotopy hypothesis. (*A*) Distribution histogram of distance between glomeruli activated by odor pairs belong to the same chemical class (*Upper*; WITHIN) or different classes (*Lower*; BETWEEN), with the data filtered at different thresholds (no threshold: T = 0; threshold at 30% maximum: T = 0.3*max; threshold at 50% maximum: right = 0.5*max). (*B*) The *P* values for the statistical tests using the Fisher combined probability test method. The *P* values for d_BETWEEN − d_WITHIN ≥ D, as a function of D, are plotted. Color lines indicate the *P* values for data filtered with no threshold (black), 30% maximum (red), or 50% maximum value (blue). Gray lines indicate the results for 12 individual experiments. (*C*) Illustration of a simplified model of chemotopy extended to the entire bulb and the overlap test (SI Materials and Methods). The olfactory bulb is treated as a sphere. *Left*: Gray-shaded area indicates where imaging experiments are conducted, and cyan-shaded area indicates the area representing a class of odorants. α_{ov} and α_{cr} denote the angle between the axis and the edge of the overlap cone and the class region, respectively. θ indicates the angle between the two axes, which will determine the degree of overlap. *Right*: Schematic showing a scenario that the glomerular sets representing different odor classes (three are shown) all overlap at the imaged area. (*D*) Probability for *N* groups chemicals (*n* = 4, 8, or 16) to overlap in the imaged area. Different curves show the size of the overlapped area, expressed as the percentage of the total sphere (black, 2%; red, 5%; blue, 10%).

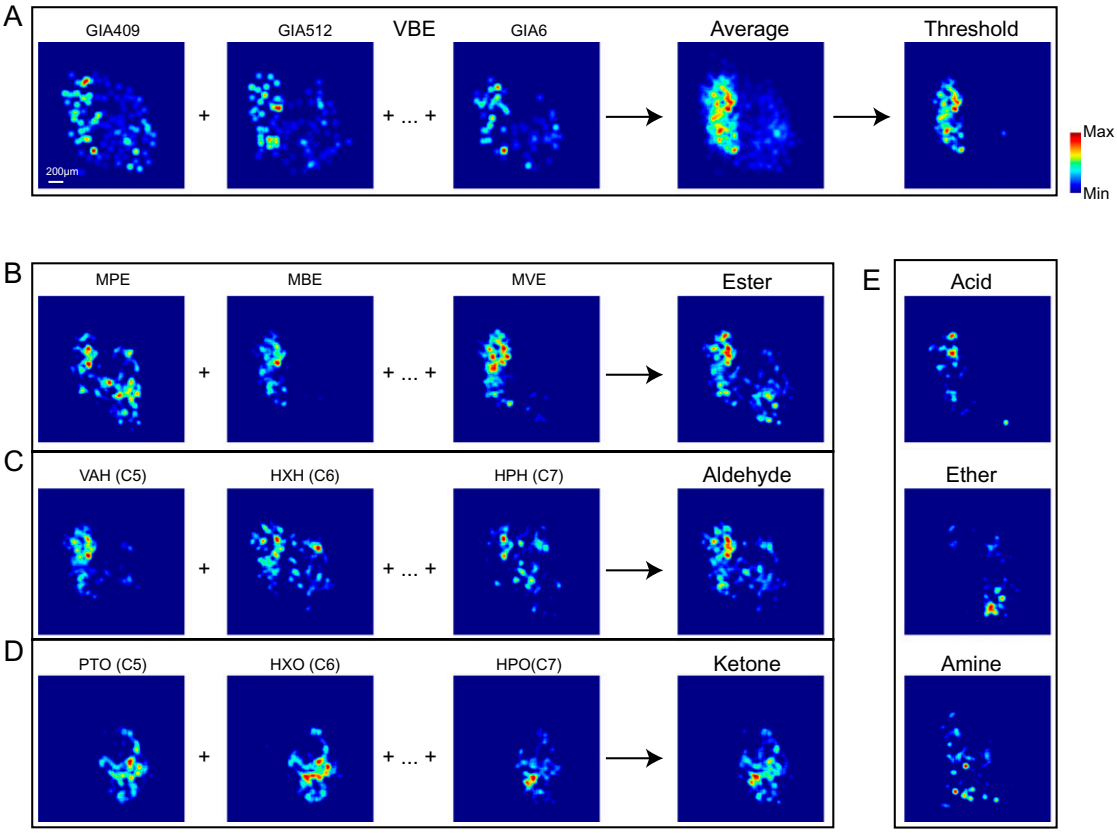

Fig. S5. Transformed representation of odors and odor classes. (*A*) Process of transforming individual experiments into a combined representation of a single odor. Vinyl butyrate (VBE) is used for illustration. Twelve separate imaging results (three shown) are rotated, aligned, averaged, and thresholded at 25% of maximum to produce an averaged representation of VBE. (*B–D*) Averaged response patterns to ester (*B*), aldehyde (*C*), and ketone (*D*) molecules as the representations of individual odor classes. Odors shown are methyl propionate (MPE), methyl butyrate (MBE), methyl valerate (MVE), valeraldehyde (VAH), hexanal (HXH), heptanal (HPH), 2-pentanone (PTO), 2-hexanone (HXO), and 2-heptanone (HPO). (*E*) Averaged patterns for acid, amine, and ether.

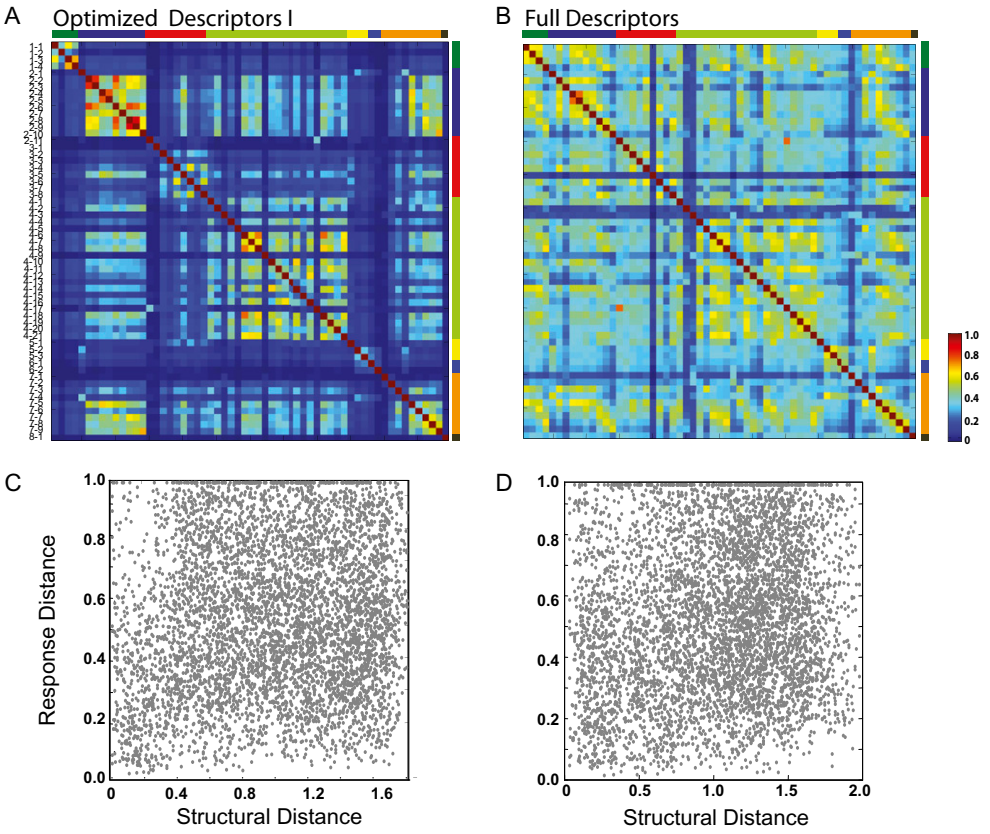

Fig. S6. Glomerular response similarity and odorant structure similarities. (*A* and *B*) Heatmap represents the pairwise correlation matrix among 59 odors using the optimized descriptor set I (*A*) or full descriptor set (*B*). Odor IDs are marked along the axes. Their names and structures can be found in Dataset S1. Odors are arranged according to chemical classes. (*C* and *D*) Scatter plots in which the similarity in glomerulus response for an odor pair is plotted against the distance between the two in chemical space described by optimized descriptor set I (*C*) or full set (*D*). Data are pooled from 12 experiments. Distances are calculated as the cosine distance for the descriptors.

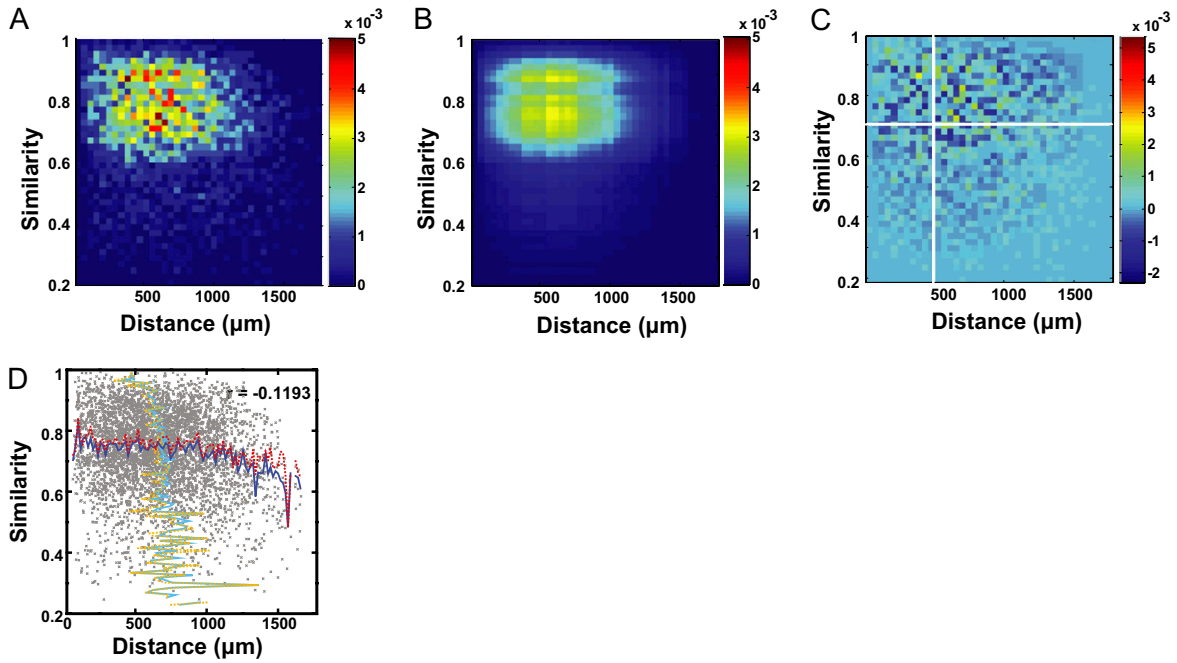

Fig. S7. Lack of correlation between glomerular tuning and physical distance for odorants delivered at high concentration. (*A*) 2D histogram showing the relationship between glomerular response similarity and physical distance for glomerular pairs. The similarities are calculated using response to odors at 2.5% S.V. Color indicates the fraction of glomerular pairs falling into the each bin. (*B*) Joint distribution of two marginal distributions for the two axes in *A* indicates the distribution under the null hypothesis. (*C*) Excess calculated from subtracting *B* from *A*. The excess of glomeruli with similarity score >0.7 and distance <500 μm only constituted 2.66% of the pairs with distance <500 μm and 0.88% of the total pairs. (*D*) *A* as scattered plot. Blue solid line shows the mean and red dashed line shows the median for distance (*x* axis). Cyan solid line shows the mean and orange dashed line shows the median values for similarity scores (*y* axis).

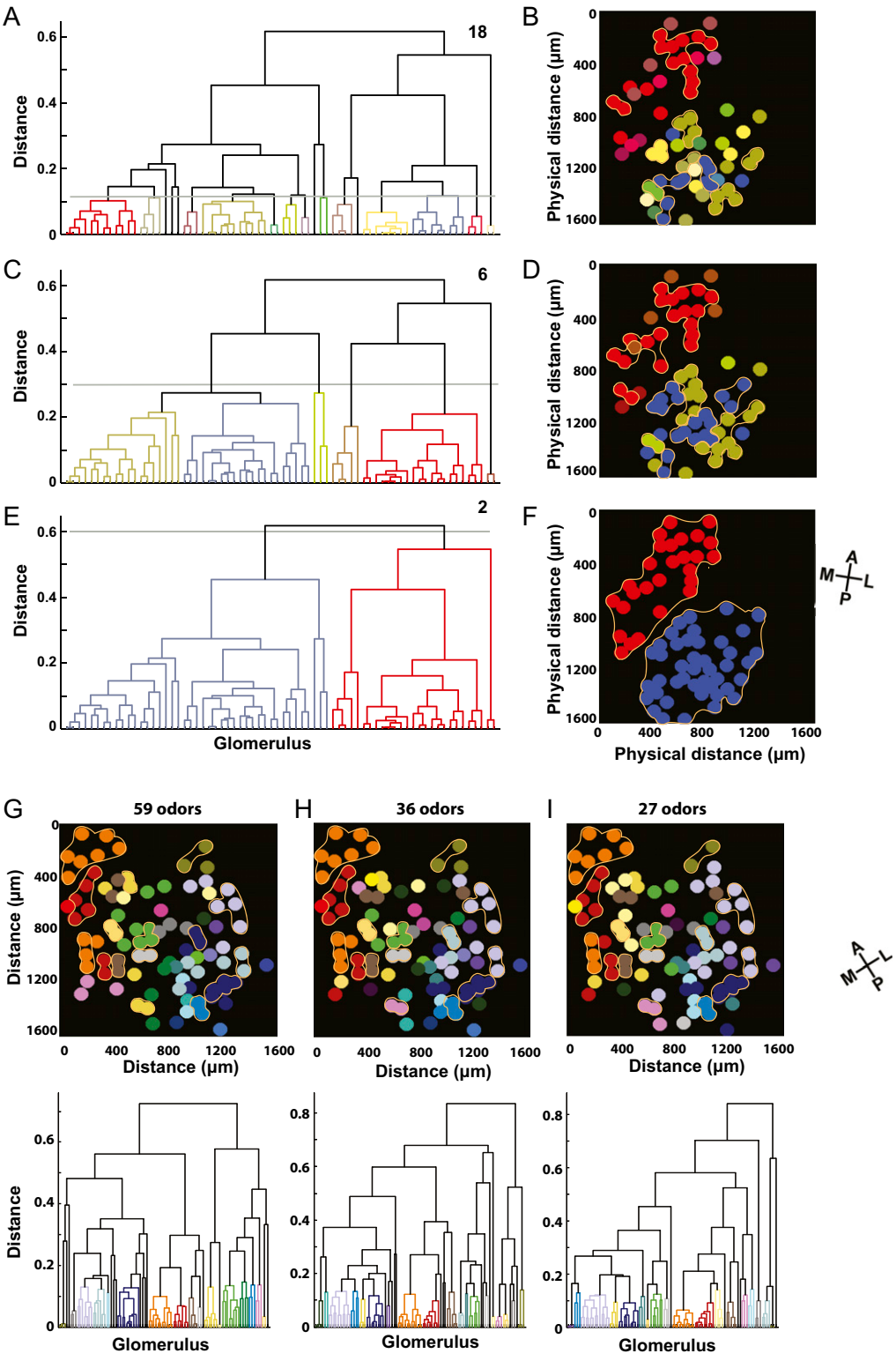

Fig. S8. Hierarchical organizations of the olfactory glomeruli. (*A*–*F*) Cluster analysis of glomerular similarity from a different experiment. (*A* and *B*) With cutoff at 0.12, the glomeruli are segregated into 18 clusters, and the glomeruli are marked for their tuning similarity. Glomeruli that are in the same tuning class and also physically close to each other are circles. (*C* and *D*) Cluster analysis with a cutoff of 0.3 segregates the glomeruli into six clusters. Some of the small clusters shown in *B* fuse into the large clusters in *D*. (*E* and *F*) Cluster analysis using a cutoff value of 0.6 segregates the glomeruli into two major clusters. (*G*–*I*) Cluster analysis of glomerular response similarity into 18 clusters using different set of odors. Maps of tuning similarity clusters onto their physical location (*Upper*) and clusters (*Lower*) for 59 odors (*G*), 36 odors (*H*), and 27 odors (*I*). Clusters that are consistent among all three odor sets are circled.

Dataset S1. Odor list

Dataset S1 (XLSX)

The list contains odor names, their functional group, and their ability to elicit response from the dorsal olfactory bulb. Odors used to map spatial representation of chemical features were listed with their odor ID and chemical structures.

Dataset S2. Numerical data for 12 separate experiments

Dataset S2 (XLS)

Numerical data for all imaging experiments used in this paper.